buildings

MDPI

Article

Study on the Flexural Behavior of Steel-Concrete Composite Beams Based on the Shear Performance of Headed Stud Connectors

Song Zhang, Yanmin Jia * and Yixing Ding

School of Civil Engineering, Northeast Forestry University, Harbin 150040, China; zhangsong@nefu.edu.com (S.Z.); demanyx@foxmail.com (Y.D.)
* Correspondence: jiayanmin@nefu.edu.cn

Abstract: Headed studs have been widely used as shear connectors in steel-concrete composite beams for a long time. Studies on the influence of the different shear properties of headed studs on the flexural behavior of the composite beams have been inconclusive. In this research, we studied the shear performance influence of headed studs by conducting static push-out tests on seven designed push-out specimens. The flexural behavior of a steel-concrete composite beam connected by studs was discussed in detail by conducting a two-point symmetric monotonic static loading test. Based on the actual situation of the composite beam test, a finite element numerical model was established and validated, in which the elastic connections units were used to simulate the studs, and the force–slip data obtained from the push-out tests were used as the constitutive model of the studs. The effects of the stud diameter, stud height, the number of studs arranged, and concrete strength on the flexural behavior of the composite beams were analyzed and compared. The results showed that the number of studs arranged had a significant influence on the flexural behavior of the composite beams, followed by the strength of the concrete. The specifications of the studs had little effect on the flexural behavior of the composite beams within the study scope using the modeling method in this paper.

Keywords: stud shear connector; push-out test; steel-concrete composite beam; flexural behavior; finite element analysis

Citation: Zhang, S.; Jia, Y.; Ding, Y. Study on the Flexural Behavior of Steel-Concrete Composite Beams Based on the Shear Performance of Headed Stud Connectors. *Buildings* **2022**, *12*, 961. https://doi.org/10.3390/buildings12070961

Academic Editor: Nerio Tullini

Received: 29 April 2022
Accepted: 3 July 2022
Published: 6 July 2022

1. Introduction

The mechanical properties of steel-concrete composite structures are affected by the properties of steel and concrete materials and determined by the shear connectors at their interface [1]. The shear connector is a key component to ensure that steel beams and concrete slabs can be subjected to force together and generate coordinated deformation in a composite beam. The headed stud connector has become the most widely used shear connector in engineering by virtue of convenient construction, reliable quality, non-directional merit, good pull-out performance, and many other unique advantages among the common shear connectors. Related studies have also been developed on the shear performance of stud connectors and the flexural behavior of steel-concrete composite beams. The push-out test, the beam test, and the finite element analysis are the three most commonly used research methods to study the working mechanism of headed studs.

Since the 1950s, many scholars, including Viest [2], Ollgaard et al. [3], Shim et al. [4], Pallares and Hajjar [5,6], Li et al. [7], and Nie et al. [8], have studied the shear performance of the stud connectors by conducting push-out tests or finite element analyses concerning the influencing parameters of the shear performance of headed studs and proposed formulas for calculating the shear capacity, which also provided an important reference for countries to formulate relevant codes. Numerous studies have shown that the factors affecting the shear performance of the studs include the diameter, height, material strength, quantity,

layout form of headed studs, strength and transverse reinforcement rate of the concrete, loading mode, etc. The shear fracture at the root of the studs is the main reason for failure in most push-out specimens. Hu et al. [9] studied the shear performance of studs based on static push-out tests using two finite element analysis software—Midas FEA and Ansys. It was concluded that the results calculated by the two software agreed with the experimental results. Huu et al. [10] established an accurate finite element model for the push-out specimen by considering various material nonlinearities to obtain the ultimate strength of the studs and investigated the effect of the changes in stud diameter and concrete strength on the capacity and the behavior of the stud connectors in the validated model. Wang et al. [11] showed that the shear bearing capacity and shear stiffness of the studs were positively correlated with the length–diameter ratio through 24 groups of push-out tests; however, the shear stiffness varied less when the length–diameter ratio exceeded 10. Meng et al. [12] suggested an analytical model for describing the shear behaviors of headed stud shear connectors by analyzing the force–slip curves and failure modes in the literature, which could predict the load–slip curve in good agreement with the existing experimental data. Wu et al. [13] showed that the shear strength of stud shear connectors could be improved by appropriately increasing the ultimate tensile strength and diameter of the studs and improving the concrete strength through push-out tests and finite element analyses.

The bending test of the composite beams is generally loaded symmetrically at two points in the span of the supported beams. Moffatt et al. [14] discussed the effect of the arrangement form of shear connectors on the force performance of steel-concrete composite beams by finite element analyses. Xing [15] showed that the change in stud diameter and height had little impact on the overall mechanical performance of the composite beams. In contrast, the decrease in stud spacing and the increase in stud columns increased the ultimate flexural capacity. Xiu et al. [16] established refined finite element models based on the push-out and beam tests and showed that the shear bearing capacity of the stud connectors obtained from the push-out tests was higher, compared with the beam tests, while the shear stiffness obtained was more conservative. Wang et al. [17] showed that decreasing the degree of shear connection could significantly reduce the ultimate bearing capacity, the ductility, and other mechanical properties of composite beams, and the failure modes were also changed. Zhang et al. [18] performed static push-out and flexural tests of composite beams on headed studs, and the results showed that the shear failure of the studs occurred in partially connected composite beams. Reducing shear connectors decreased the composite beams' initial stiffness and bearing capacity and increased the relative slip in the interfaces. Using composite beam tests and finite element analyses, Sangeetha et al. [19] showed that the composite beams arranged with fewer connectors had greater deflection and slip. Ding et al. [20] investigated the shear performance of steel-concrete composite beams connected with studs through finite element numerical analyses based on steel-concrete composite beam tests, derived the bounded shear-to-span ratios of the composite beams subjected to bending damage or bending–shear damage, and proposed a formula for calculating the shear strength of the composite beams.

Some achievements have been made in the shear performance of stud connectors or flexural performance of composite beams, but there is much yet to explore. Studies have been inconclusive regarding the flexural behavior of composite beams based on the influence of different shear properties of headed studs. This paper focused on the shear performance of stud connectors and the flexural behavior of steel-concrete composite beams. The influence of the shear performance of headed studs was studied by conducting static push-out tests on three groups of seven designed push-out specimens. The flexural behavior and failure mechanism of a steel-concrete composite beam connected by studs were investigated in detail by conducting a two-point symmetric monotonic static loading test. Based on the actual situation of the composite beam test, the finite element numerical model was established and validated, in which the elastic connection units were used to simulate the studs, and the force–slip data obtained from the push-out test were used as

the constitutive model of the studs. The effects of the stud diameter, stud height, number of studs arranged, and concrete strength on the flexural behavior of composite beams were analyzed and compared.

2. Push-Out Tests

The push-out test is the most common method to determine the shear performance of studs. In this study, a push-out test was proposed to obtain the force–slip curves of the stud connectors and study the variations in the studs' shear performance, which provided a basis for the subsequent simulation of the stud connectors in the finite element analyses of the composite beams.

2.1. Set-Up of the Push-Out Test

Considering the variations in concrete strength, stud diameter, and stud height, three groups of seven push-out specimens were designed and fabricated with reference to the construction requirements of Annex B in Eurocode 4 [21]. The details of the specimens are presented in Figure 1. The parameters and grouping of the specimens are shown in Table 1.

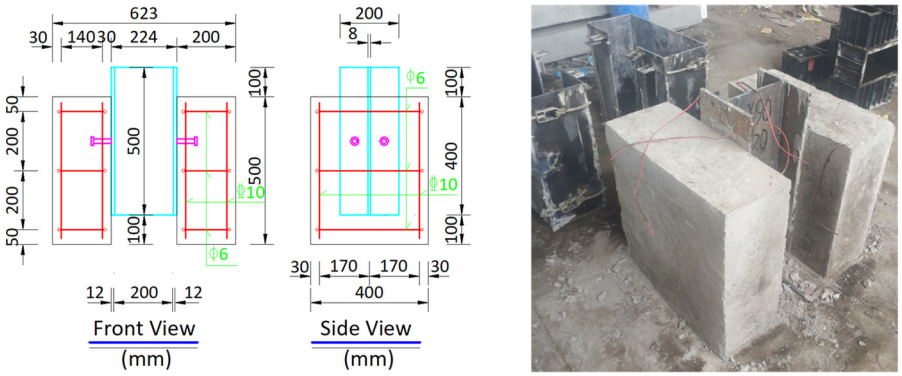

(**a**) (**b**)

Figure 1. Push-out specimens: (**a**) design dimensions; (**b**) actual photograph.

Table 1. Parameters and grouping of specimens.

Groups	Specimens	Stud Diameter (mm)	Stud Height (mm)	Design Strength of Concrete (MPa)	Measured Strength of Concrete (MPa)	Variable Parameters
R	C40D16H90	16	90	40	39.7	—
C	C30D16H90	16	90	30	32.3	Concrete Strength
	C50D16H90	16	90	50	49.8	
D	C40D13H90	13	90	40	42.2	Stud Diameter
	C40D19H90	19	90	40	39.2	
H	C40D16H60	16	60	40	38.5	Stud Height
	C40D16H120	16	120	40	39.5	

The materials and fabrication of the specimens were in accordance with the requirements of Chapter 3 and Section 9.1 in the Chinese 3362 code [22] and Chapter 3 in the Chinese 10433 code [23]. The steel beam was fabricated with Q355B steel plates welded by laser cutting, and the headed studs were made of ML15 steel. The materials of longitudinal reinforcement and stirrup of the concrete slab were HRB400 and HPB300, respectively. Three 150 × 150 × 150 mm cube specimens were made of the same concrete during concreting and then cured under the same conditions as the push-out specimens and were measured using a TYA-2000 electrohydraulic pressure tester on the test day. The measured compressive strength of concrete cubes is shown in Table 1.

The static push-out tests were performed with a PWS-30000 electrohydraulic servo pressure testing machine. The schematic diagram and actual photograph of the test loading

device are shown in Figure 2. The tests were loaded by controlling displacement with a constant loading rate of 0.03 mm/min, which referred to the provisions of Chapter 4 in the Japanese Society of Steel Construction (JSSC) [24].

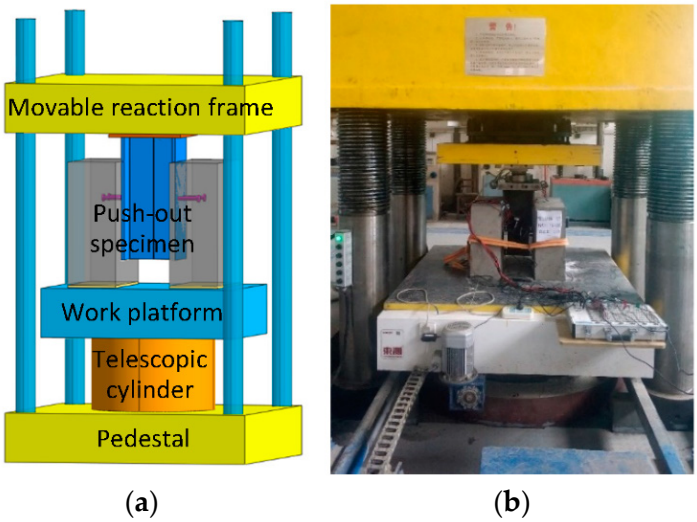

Figure 2. Loading device for push-out tests: (**a**) schematic diagram; (**b**) actual photograph.

The relative slip between the steel beam and the concrete slab was measured by arranging displacement sensors (YHD-20 type with a range of 20 mm and an accuracy of 0.1 mm) near the equivalent height of each stud.

2.2. Results of the Push-Out Test

All specimens were damaged due to a shear fracture at the root of the studs, and the concrete at the lower edge of the studs was also partially crushed.

The force–slip curves of a single stud obtained from the push-out tests are shown in Figure 3. Table 2 lists the test results of the single stud capacity of specimens. One-fourth of the maximum force was adopted as the force of the single stud, and the average relative slip at four positions was taken as the slip data in the curves.

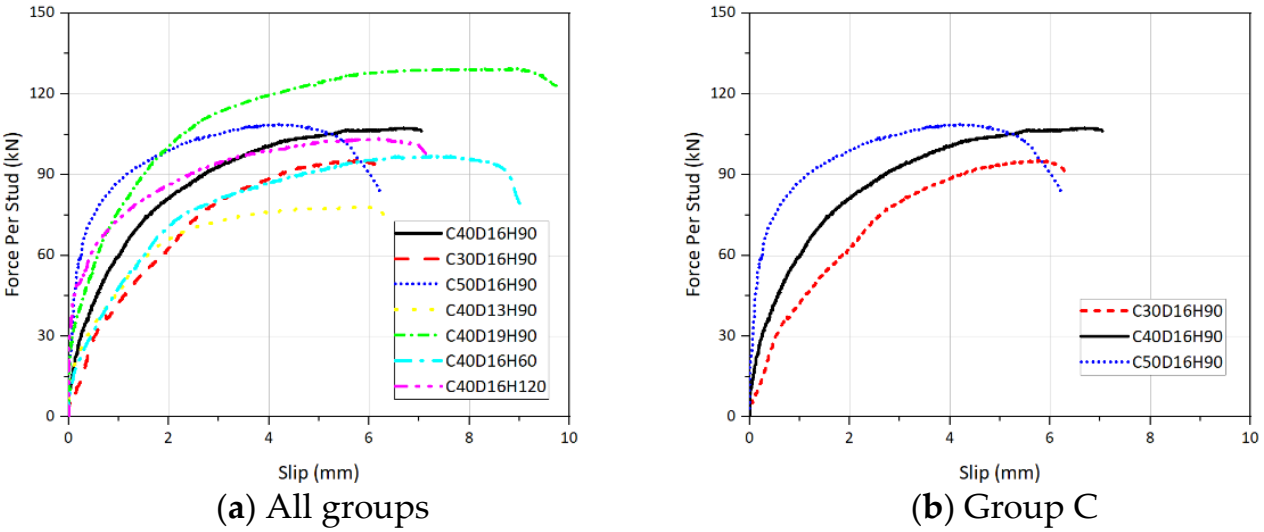

Figure 3. *Cont.*

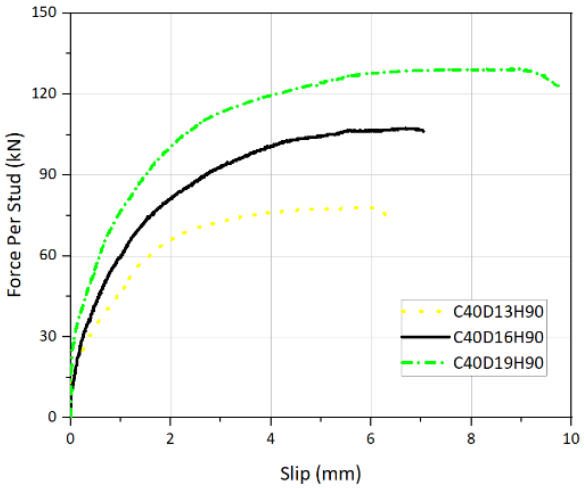

(**c**) Group D

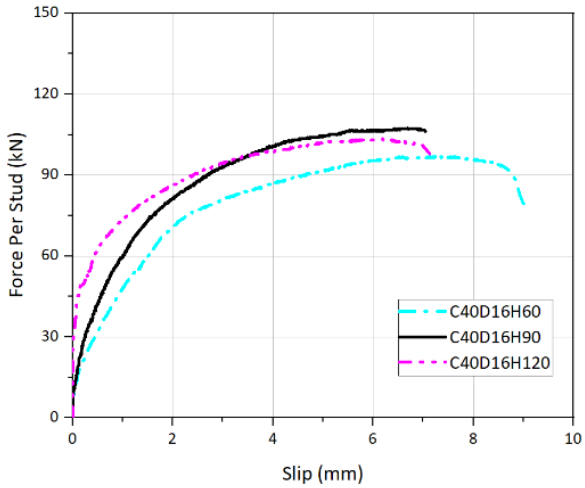

(**d**) Group H

Figure 3. Force–slip curves: (**a**) all of seven push-out specimens; (**b**) Group C: different strength grades of Concrete; (**c**) Group D: different stud diameters; (**d**) Group H: different stud heights.

Table 2. Test results of shear capacity of a single stud.

Groups	Specimens	Ultimate Shear Capacity (kN)	Ratio to Reference Group
R (Reference)	C40D16H90	107.3	100%
C (Concrete)	C30D16H90	95.3	−11%
	C50D16H90	108.9	+2%
D (Diameter)	C40D13H90	78.1	−27%
	C40D19H90	129.6	+21%
H (Height)	C40D16H60	97.0	−10%
	C40D16H120	103.6	−3%

In the analysis of the push-out test, the force–slip curves were the most critical characteristic curves, as they could reflect the overall change in the shear connector under load. The mechanical properties of the studs, such as shear capacity, ultimate slip, and shear stiffness, could be obtained from the analysis of the force–slip curves.

There was no unified conclusion on the value of the shear stiffness of the studs, but the slope of the force–slip curves of the specimens in the elastic phase as the shear stiffness was generally accepted. As shown in Figure 3 and Table 2, the shear stiffness of the stud had obvious positive correlations with concrete strength, stud diameter, and stud height.

The shear capacity of the stud increased with the increase in the stud diameter. Compared with 13 mm diameter studs, the shear capacity of 16 mm and 19 mm diameter studs increased by 27% and 48%, respectively, and the corresponding ultimate slip also increased significantly. After increasing the height of the studs from 60 mm to 90 mm, the ultimate shear capacity of the stud increased by 10%, but the ultimate slip was significantly reduced; after increasing the height from 90 mm to 120 mm, the ultimate shear capacity and ultimate slip remained basically the same. The ultimate shear capacity of the studs increased by 11%, raising the concrete grade from C30 to C40 but only 2% from C40 to C50.

In summary, the shear performance of the stud was significantly affected by the changes in the above three parameters. However, the influence of the above factors on the flexural performance of the composite beams was not definitive. Therefore, further research was necessary.

3. Bending Test of the Composite Beam

The beam test is a common method to study the actual mechanical performance of studs. In this study, a two-point symmetrical monotonic static loading test was conducted on a steel-concrete composite beam connected with studs to analyze and study the flexural behavior and failure mechanism, which also provided a basis for the finite element numerical analyses of the composite beams.

3.1. Set-Up of the Composite Beam Test

The design of the specimen for the steel-concrete composite beam test was based on the Liuganyingzi Bridge project in Chaoyang, Liaoning Province, China. The principle of scaling was to maintain the strength of the materials, boundary conditions, and longitudinal stud spacing constant, and to reduce the cross-sections of the concrete slab and the I-beam by the inertia moment similarity constant of 0.0081, corresponding to a geometric scaling-down constant of 0.3. The span of the bridge was arranged as a 4 × 13 m simply supported steel-concrete composite beam, with seven beams arranged horizontally at a spacing of 1900 mm. The steel beams adopted 708 × 304 × 15 × 28 mm H-beams, and two rows of φ22 × 100 mm studs were arranged at a spacing of 110 mm on the upper flange of the steel beams, and the thickness of the concrete deck slab was 220 mm.

The design of the composite beam specimen referred to the C40D16H60 specimen in the push-out test; the materials, fabrication, and curing conditions were designed accordingly as well. The calculated span of the composite beam was 3770 mm, the concrete slab thickness was 100 mm, and the total beam height was 306 mm. A total of 16 studs (φ16 mm × 60 mm) were arranged in a single row on the centerline of the steel flange plate, and 1 stud per side was welded on the end of the steel web above the fulcrums, totaling 20 studs for the whole beam.

The loading device is shown in Figure 4. The loading components for the composite beam test from top to bottom were reaction frame, load sensor, lifting jack, distribution beam and distribution support, steel plate, knife-edge support, rolling support, and steel buttress.

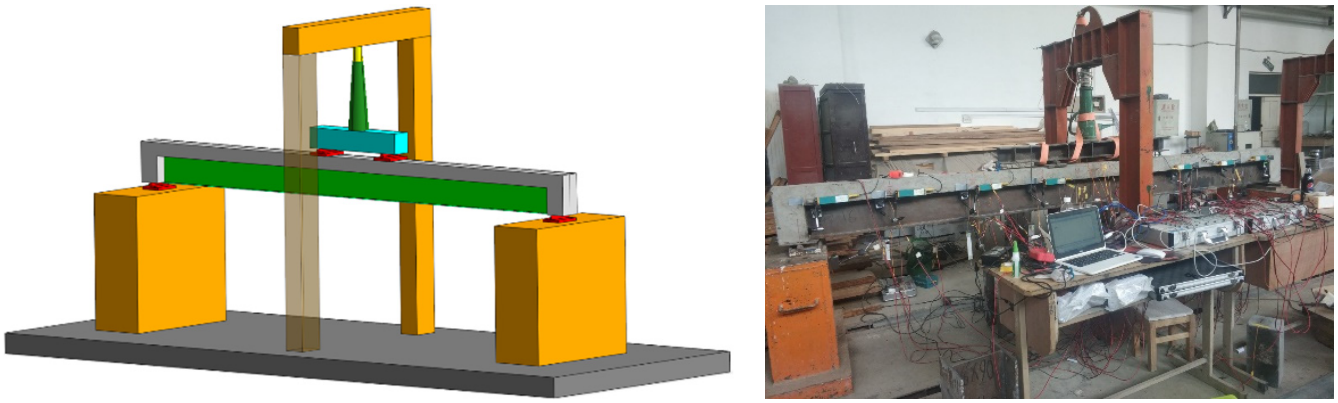

(**a**) (**b**)

Figure 4. Loading device for the composite beam test: (**a**) schematic diagram; (**b**) actual photograph.

During the loading, the data such as force, deflection, interface slip, and strain of steel beam and concrete were measured to analyze the working mechanism of the composite beam. The layout positions of the measuring points are shown in Figure 5a, and the naming rules for the strain measurement points in Figure 5b are as follows: calculated span (L), loading point (P), concrete (C), steel beam (S), upper (U), middle (M), lower (D), web of the steel beam (W).

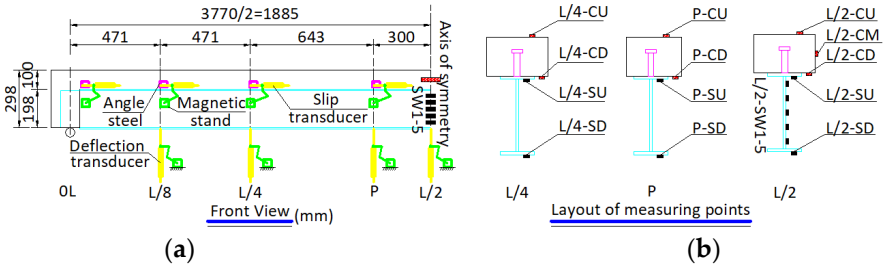

Figure 5. The layout of measuring points of the composite beam: (**a**) front view; (**b**) cross-section.

The loading method of the two-point symmetrical monotonic static loading was adopted in the bending test of the composite beam, and the center spacing of loading points (pure bending section) was 600 mm. The tests were loaded by controlling force with each load increment of 5 kN for 3 min. We observed and recorded the test phenomenon and crack development of the composite beam during the load duration. As with the push-out test, preloading should be performed before formal loading. The specimen was considered damaged when the load reached the limit value, and excessive deformation or cracks occurred in the composite beam specimen; it was then unloaded at 50 kN per level until the end of the test.

3.2. Test Results of the Composite Beam

3.2.1. Failure Mode

The final failure mode of the composite beam was the bending failure in the pure bending section and the shear failure at the fulcrums, as shown in Figure 6. Large plastic deformation occurred in the composite beam. There were multiple horizontal penetration cracks in the pure bending section of the concrete slab, while obvious inclined cracks appeared near the fulcrums and extended to the corner of the concrete slab. The lower flange of the steel beam yielded under the loading point, but damage to the studs was not observed.

Figure 6. Failure form: (**a**) left fulcrum; (**b**) pure bending section; (**c**) right fulcrum.

3.2.2. Deflection

Since the specimen dimensions, loading points, and arranged measurement device were symmetrical, only the left span of the composite beam is shown for analysis, and the average values of the symmetrical measurement device were adopted for deflection, slip, and strain.

Combined with the test phenomenon and Figure 7a, the loading process of the composite beam specimen was divided into four stages: elastic stage (0–40 kN), elastic–plastic stage I (40–110 kN), elastic–plastic stage II (110–140 kN), and descending stage (>140 kN). The details were as follows:

(1) In the elastic stage, the stress of the composite beam was relatively minor, the interface slip had not yet occurred, and the deflection increased linearly with the load. The overall working performance of the composite beam was ideal.

(2) When the load exceeded 40 kN, there were minor inflection points in the curves, the interface slip began to develop, the deflection increased approximately linearly with a greater growth rate, the steel beam was still mainly elastic, and the plastic deformation began to develop.

(3) Since the load reached approximately 110 kN, the development of plastic deformation of the composite beam was accelerated, and cracks near the mid-span and the fulcrums started to develop.

(4) After the load exceeded 140 kN, the load was difficult to continue to increase, but the growth rate of deflection continued to accelerate. Meanwhile, several horizontal cracks in the concrete began to penetrate, the concrete near the fulcrums was crushed, and the cracks widened. The composite beam specimen was declared damaged.

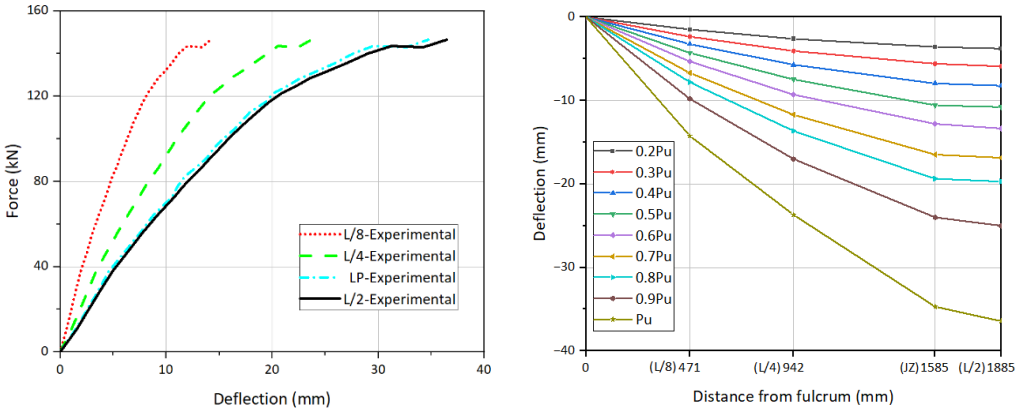

(**a**) (**b**)

Figure 7. Deflection curves: (**a**) force–deflection curves; (**b**) deflection along the beam.

The distribution diagram of the deflection along the beam length under typical loads was made, as shown in Figure 7b, in which Pu (146.5 kN) was the ultimate load of the specimen. As shown in Figure 7b, the deflection distribution curves were close to a parabola; the maximum deflection appeared at mid-span. Before the load reached 0.8 Pu, the deflection of the composite beam increased slowly and uniformly with the load. The deflection grew significantly faster after exceeding 0.8 Pu, and the deflection grew at a more substantial rate since 0.9 Pu. Since the load reached the Pu, the deflection increased sharply, and the composite beam could be considered a failure.

3.2.3. Interface Slip

The force–slip curves along the composite beam length are shown in Figure 8.

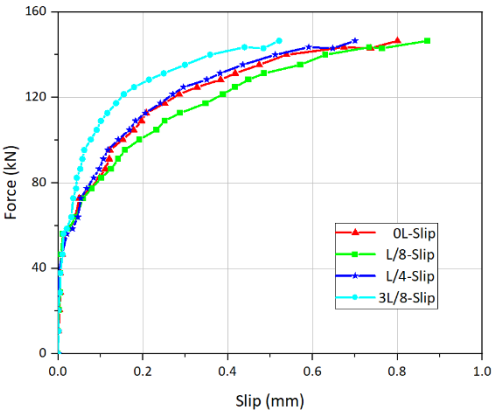

Figure 8. Force–slip curves of the interface of the composite beam.

As shown in Figure 8, the relative slip of the interface developed from 40 kN, the slip was generally minor, and the growth of the slip curves was gentle. When the force exceeded approximately 115 kN, the slip rate increased significantly, and the difference in the slip at different positions increased significantly. The relative slip at L/8 was the largest but did not exceed 1 mm, followed by the slip at the fulcrum and L/4, and the relative slip at 3L/8 near the mid-span was the smallest. The maximum sliding position did not appear near the fulcrums, which could have been due to the setting of the studs on the steel beam web above the fulcrums. Since the force exceeded 130 kN, the force approached the ultimate load, and the growth rate of the slip was further accelerated, which was due to the increase in and development of cracks and the rapid decline in the overall stiffness of the composite beam specimen. The development of force–slip curves also confirmed the analysis of force–deflection curves in this study.

3.2.4. Strain of Steel Flange and Concrete Slab

The force–strain curves of the concrete slab are shown in Figure 9. As shown in Figure 9a, the concrete top surface was always compressed during loading, and the force–strain curves of the concrete top surface at L/4 were close to linear, which had still been in the elastic stage when the specimen had been damaged. The strain curves at P and L/2 in the pure bending section coincided during loading. In addition, the curves were approximately linear until the loading reached 105 kN, after which the strain growth rate gradually increased. At a force of approximately 130 kN, the strain of concrete reached the yield strain.

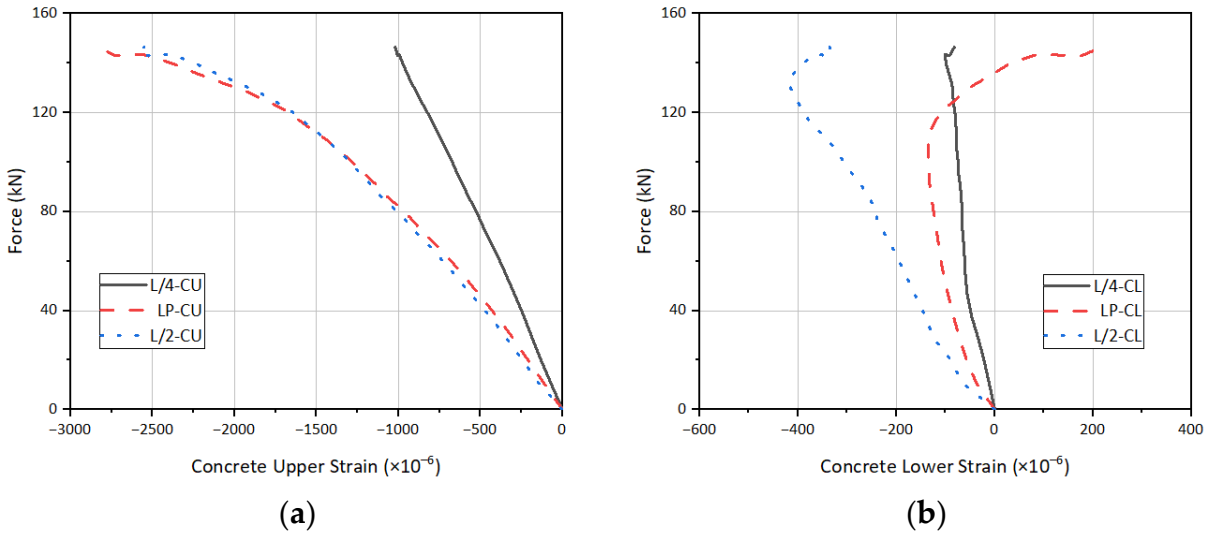

Figure 9. Force–strain curves of concrete slab: (**a**) upper surface; (**b**) lower surface.

As shown in Figure 9b, the strain on the lower surface of the concrete at L/4 was minor and always compressed. The concrete strain at P changed from negative to positive when the force reached 140 kN; that is, the concrete changed from compression to tension. Since the strain of the upper flange of the steel beam remained negative, we speculated that the neutral axis might still have been in the web of the steel beam due to the development of cracks that reduced the stiffness of the concrete, and the concrete at the measuring point was in the cantilever state, which led to the tensile stress at the lower edge of the concrete under the transverse force of the distribution support. This conclusion could be supported by the fact that the upper flange of the steel beam at L/2 was always in the compression state during the loading process.

The force–strain curves of the steel beam in the composite beam specimen are shown in Figure 10. As shown in Figure 10a, the upper flange of the steel beam along the beam length was always under compression, and the strain was minor, which was far from reaching the yield strength of the steel. The strain at P and L/2 coincided, and the strain at

the upper flange of the steel beam at P was slightly larger under the same force in the later stages of loading.

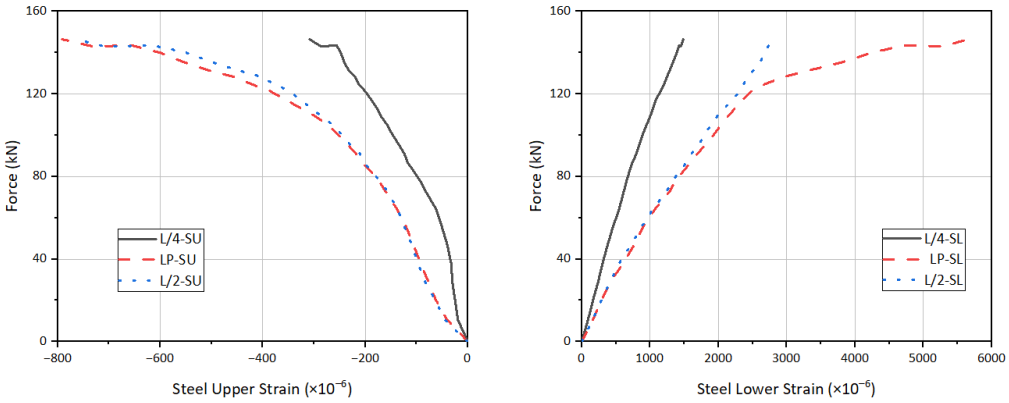

(**a**) (**b**)

Figure 10. Force–strain curves of steel flange: (**a**) upper flange; (**b**) lower flange.

As shown in Figure 10b, the lower flange of the steel beam was always under tension. The strain at L/4 was minor, and the curves were approximately linear, which could be considered that the measuring point was always in the elastic stage. The strain curves at P and L/2 coincided in the early stage of loading as the beam was in the elastic stage or the plastic deformation was minor. With the loading exceeding 80 kN, the strain at P increased slightly faster than that at L/2. Since the force reached 100 kN, the strains at both locations reached the yield strain of steel successively. Then, the strain growth rate at P accelerated. When loaded to 140 kN, the strain growth rate increased rapidly. The strain at the lower edge of the steel beam at P far exceeded the limit strain, and the composite beam specimen was declared a failure. The lower flange of the steel beam at P was damaged first, which led to the damage of the whole beam.

3.2.5. Strain along the Section Height at L/2

The force–strain curves of the steel beam web at L/2 are shown in Figure 11a, and the strain curves along the section height at L/2 under typical force are shown in Figure 11b.

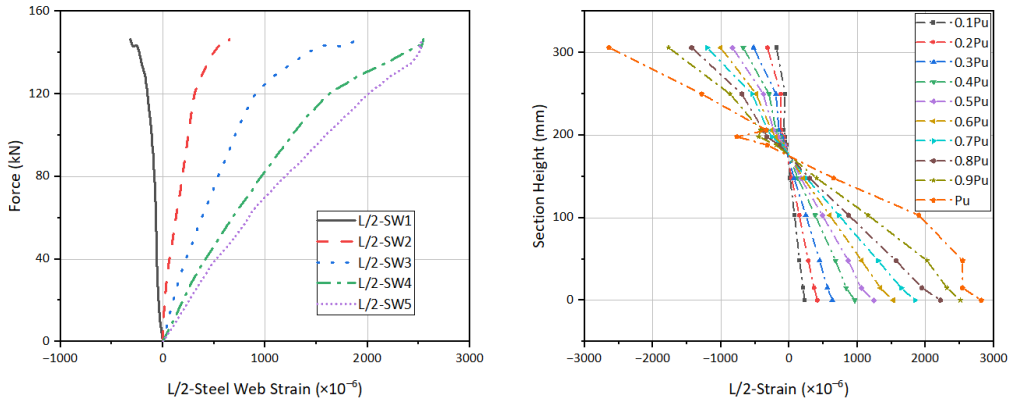

(**a**) (**b**)

Figure 11. The strain of mid-span section in the composite beam: (**a**) force–strain curves of steel web; (**b**) the strain across the section height.

As shown in Figures 5a and 11a, the upper SW1 measuring point at the steel web was always under compression, the other four measuring points were always under tension, and the point with the section strain of zero, that is, the neutral axis of the composite beam, was located between SW1 and SW2. Before the force was 110 kN, the strain of all measuring

points increased linearly with the load, and the strain of the measuring point closer to the upper flange was less. Since the force exceeded 110 kN, the strain growth rate of all measuring points increased significantly. The lowest measuring point of SW5 reached yield strain first, and then the measuring points of SW4 and SW3 successively reached the steel yield strain, while the other two measurement points did not yield.

As shown in Figure 11b, the strains of the upper flange of the steel beam and the concrete slab were approximately equal at the intersection before 0.8 Pu (approximately 117 kN), which indicated that the studs could effectively transfer the force from the concrete slab to the steel beam. In addition, the two could deform and work together better. The cross-sectional strain curves of the composite beam at L/2 were approximately linear, which conformed to the plane section assumption. As the loading continued, the strain difference between the two at the interface gradually became larger, the strain growth rate of all measuring points accelerated, and the concrete's upper edge and the steel beam's lower flange reached the corresponding yield strain in succession. The position of the neutral axis of the composite beam was approximately 180 mm from the bottom of the beam.

4. The Finite Element Analysis (FEA) of the Composite Beams

4.1. Development of Finite Element Model

Although the experimental research method can best reflect the actual situation of the specimens, it has certain limitations, such as a long research period, expensive cost, etc. The finite element analysis method can significantly compensate for these shortcomings. Based on the actual situation of the composite beam test, the transverse 1/2 finite element model of the composite beam was established using Midas FEA NX finite element software, considering the symmetry of the beam test.

The concrete slab was meshed by 3D solid units, whereas the steel beam was meshed by 2D plate units. The mesh nodes on the contact surfaces between the steel beam and concrete were fully coupled, and elastic connection elements were set at the actual positions of 20 studs in the composite beam to simulate the studs. General contact pairs were manually set on the concrete and steel beam's coupling contact surfaces. The contact surfaces could be in contact or separated before and after the analysis without considering the friction coefficient of the contact surface.

The studs were simulated by inputting the nonlinear elastic function curves to define the mechanical parameters of the elastic connection units in the model. The materials, fabrication, and curing of the composite beam specimen were the same as those of the specimen of C40D16H60 in the push-out test. Therefore, the force–slip curves of the C40D16H60 specimen were used as the nonlinear elastic function curves of the stud, as shown in Figure 12.

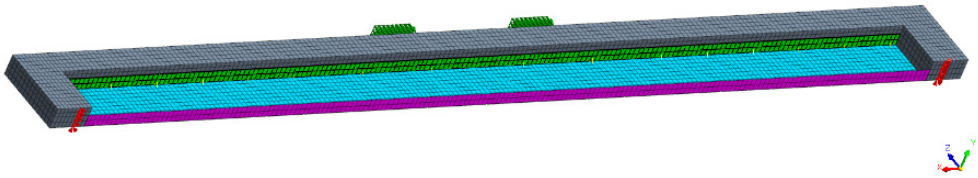

Figure 12. Established finite element model.

The 3D unit surface load of −5 MPa in the Z direction was set at the loading point of the composite beam in the model, and the total equivalent load of the whole beam was 240 KN. The boundary conditions of the composite beam specimen were simulated as a simply supported beam, according to the test, with the left fulcrum fixed and the right slidable, and the established finite element model is shown in Figure 12.

The nonlinear static analysis was adopted in the finite element model. The external load was divided into 100 incremental steps. The criterion of a displacement variation less than 0.03 mm was taken as the convergence standard of each incremental step analysis. Different iterative methods for updating stiffness greatly impact the calculation accuracy and

operation speed during the solution process. The software provided four iterative methods for different situations, including the initial stiffness method, the arc–length method, the Newton–Lapson method, and the modified Newton–Lapson method. This model adopted the default iterative method in the software program, which could automatically convert the iteration method for the calculation requirement.

4.2. The Constitutive Relation

The selection of the material constitutive model was crucial, as it would directly affect the calculation results in the nonlinear finite element analysis. Without considering the influence of ordinary reinforcement, the constitutive relations and mechanical property parameters of concrete and steel beams selected in the model are described in what follows.

The constitutive relationship of concrete under tension and compression load was adopted from the constant model in the smeared crack model provided by the program, as shown in Figure 13a,b. The compressive strength of the concrete was adopted from the measured cube compressive strength value in Table 1, and other parameters such as tensile strength, elastic modulus, and Poisson's ratio were taken according to the Chinese 3362 code [22], as shown in Table 3.

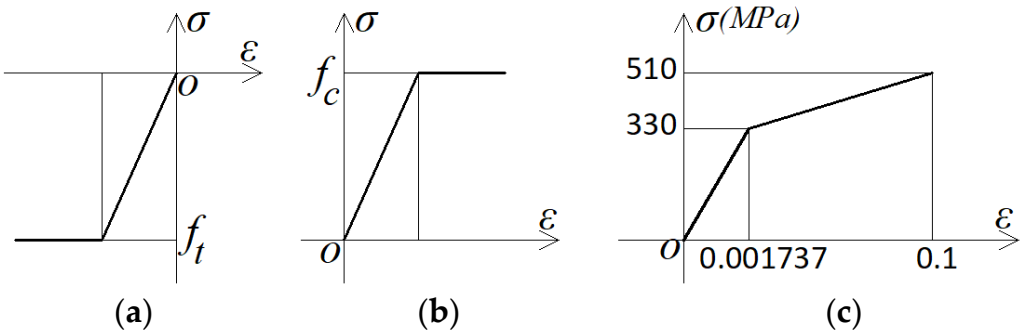

Figure 13. Constitutive relationship: (**a**) the compression model of concrete; (**b**) the tension model of concrete; (**c**) Q355B steel plate.

Table 3. Material properties of concrete in FEA models.

Concrete Grade	Compressive Strength (MPa)	Tensile Strength (MPa)	Elastic Modulus (MPa)	Poisson Ratio
C30	32.3	2.01	3.00×10^4	0.2
C40	40.0	2.40	3.25×10^4	0.2
C50	49.8	2.65	3.45×10^4	0.2

The constitutive relationship of Q355B steel adopted the bilinear Von Mises model, in which the elastic modulus was 1.9×10^5 MPa in the elastic stage (within 330 MPa) and 2.18×10^4 MPa in the plastic stage (beyond 330 MPa). The hardening curves for Q355B steel adopting the Von Mises constitutive model are shown in Figure 13c.

4.3. Validation

The finite element model of the composite beam was solved, and the force–deflection curves of the composite beam at L/8, L/4, and L/2 were extracted and compared with the corresponding force–deflection curves obtained from the composite beam test, as shown in Figure 14. The deflection difference at a typical load between the FEA and the beam experiment is shown in Table 4.

As shown in Figure 14 and Table 4, the force–deflection curves of both were relatively close. Compared with the test values, the deflection calculation difference was within 10%, and the deflection difference at L/4 and L/2 was controlled within a 5% limit. The finite element model was in good agreement with the test results, and the development trend was similar, especially for the deflection calculation at L/2 of the composite beam, with high

accuracy. The established finite element model was considered reasonable and reliable, and it could be used for further research and analysis of the composite beam.

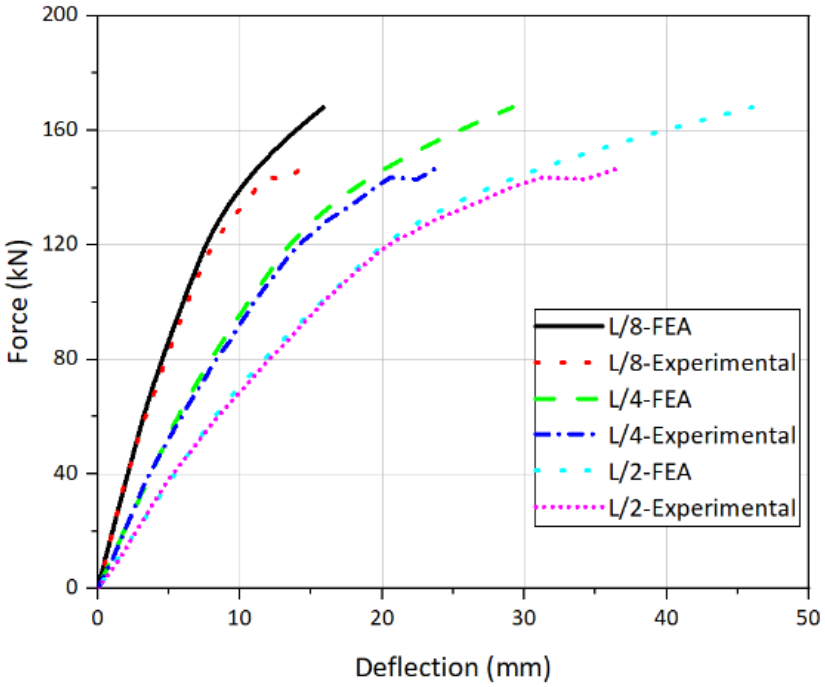

Figure 14. Comparison of force–deflection curves between experiment and FEA.

Table 4. The relative difference in deflection at typical forces.

Typical Forces (kN)	29	59	82	100	109	122	131	140	146.5
Deflection difference at L/8 (%)	−8	−10	−13	−6	−5	−1	−4	−4	−11
Deflection difference at L/4 (%)	−4	−5	−8	0	−1	4	1	1	−2
Deflection difference at L/2 (%)	−2	−2	−4	4	3	7	3	3	−1

4.4. Analysis under Different Parameters

4.4.1. The Number of the Studs

Based on the validated finite element model, the finite element models with 16, 8, 4, and 2 studs arranged on the upper flange of the steel beam were obtained by deleting the elastic connection units used to simulate studs in the model, and the other parameters remained unchanged.

For the convenience of analysis, the load corresponding to the stress of the lower flange of the steel beam at L/2 and 330 MPa was defined as the yield load of the composite beam, and the load corresponding to 1/50 (75.4 mm) of the calculated span was defined as the ultimate load of the composite beam. The force–deflection curves of the composite beam at L/2 were obtained by solving the model according to the above four groups of the stud layout, as shown in Figure 15. The calculated values of yield load and ultimate load of the composite beams with different numbers of studs are shown in Table 5.

As shown in Figure 15 and Table 5, the flexural capacity of the composite beam was positively related to the number of studs arranged. Compared with the model with only two studs, the yield load and ultimate load of the other three groups of the composite beam increased by approximately 9% on average; that is, increasing the number of studs could increase the flexural capacity of the composite beams, but the growth rate of flexural capacity gradually decreased.

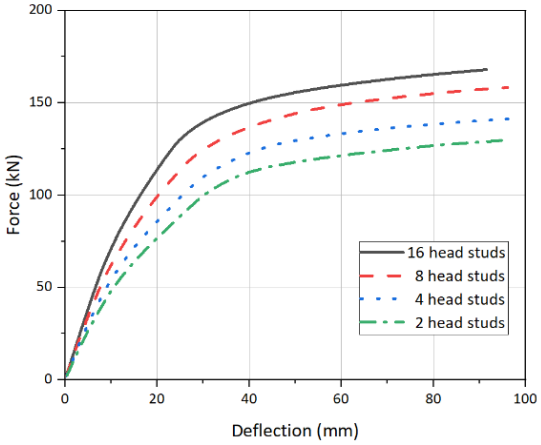

Figure 15. Force–deflection curves for different numbers of the studs.

Table 5. Comparison of calculated capacity with different numbers of the studs.

Number of the Studs	16		8		4		2	
	Force	Relative Ratio	Force	Relative Ratio	Force	Relative Ratio	Force	Relative Ratio
Yield load (kN)	139.2	1.26	129.6	1.17	117.6	1.07	110.4	1
Ultimate load(kN)	163.2	1.31	153.6	1.23	136.8	1.10	124.8	1

4.4.2. Concrete Strength

Based on the validated finite element model, the force–deflection curves of the composite beam model with different concrete strengths were calculated by changing the mechanical properties of the concrete, as shown in Figure 16. Table 6 lists the comparison of yield strength and ultimate strength of the composite beams under different concrete strengths. The performance parameters of concrete are shown in Table 3.

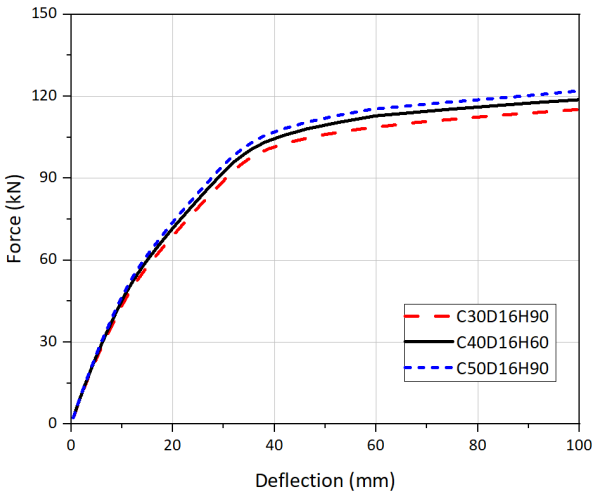

Figure 16. Force–deflection curves for different strengths of concrete.

Table 6. Comparison of calculated capacity with different strengths of concrete.

Concrete Grade	C30		C40		C50	
	Force	Relative Ratio	Force	Relative Ratio	Force	Relative Ratio
Yield load (kN)	103.2	1.00	105.6	1.02	108.0	1.05
Ultimate load (kN)	111.2	1.00	115.6	1.04	118.6	1.07

As shown in Figure 16 and Table 6, the flexural capacity of the composite beams was weakly positively correlated with the concrete strength. Increasing the concrete strength had a certain contribution to the improvement of the capacity of the composite beams. Improving the concrete strength from C30 to C40 or C50, the yield load of the composite beam increased by only 2% and 3%, respectively, and the ultimate load by only 4% and 3%, respectively.

4.4.3. Stud Diameter and Stud Height

The FEA model with only two studs was used to analyze the impact of the change in the stud specifications based on the validated composite beam model.

While other parameters remained unchanged in the model, the force–slip curves of Groups D and H in the push-out tests were used as the nonlinear elastic function of the elastic connection units to simulate the studs, as shown in Figure 3c,d, in order to study the effects of the stud specifications on the capacity of the composite beams. The force–deflection curves of the composite beam calculated by using various stud specifications are shown in Figure 17. The comparison of calculated values of yield load and ultimate load of models under different stud specifications is shown in Table 7.

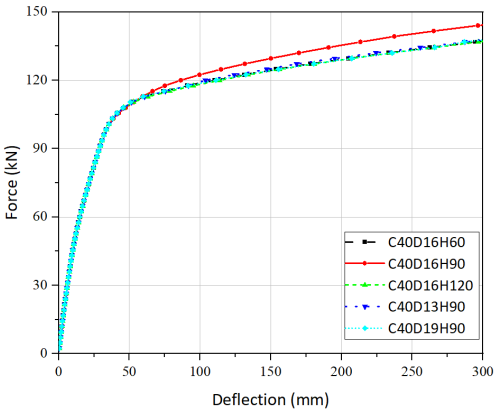

Figure 17. Force–deflection curves for different Specifications of the studs.

Table 7. Comparison of calculated capacity with different specifications of the studs (unit of force: kN).

Specifications of the Studs	C40D16H60		C40D16H90		C40D16H120		C40D13H90		C40D19H90	
	Force	Ratio	Force	Ratio	Force	Ratio	Force	Ratio	Force	Ratio
Yield load	98.4	1.00	98.4	1.00	98.4	1.00	98.4	1.00	98.4	1.00
Ultimate load	115.2	1.00	117.6	1.02	115.2	1.00	115.2	1.00	115.2	1.00
Stud force at beam yield	31.2	1.000	30.8	0.987	31.3	1.003	31.3	1.003	33.0	1.058
Stud force at beam limit	40.2	1.000	45.5	1.132	39.3	0.978	40.0	0.995	34.4	0.856

As shown in Figure 16 and Table 7, the calculated force–deflection curves of the composite beam with different specifications were similar, and changing the diameter and height of the studs had little effect on the deflection, ultimate load, and yield load at L/2 of the composite beams, which could even be overlooked. The maximum force on the analyzed studs did not exceed 46 kN, and the maximum stud slip did not exceed 1.5 mm, which was far from the shear load capacity and ultimate slip of the studs. Due to these analysis results, it was prudent to conclude that by adopting the finite element model in the paper for the five stud specifications mentioned, changing the stud diameter or height had little effect on the flexural capacity of the composite beams when the studs reached a certain degree of connection.

These conclusions may not be wholly accurate to the actual project, as the studs with diameter or height values that are too low could affect the force performance of the

composite beams. This may have been because the composite beam reached a yield or ultimate load range, while the forces of the studs were still in a linear growth stage. The force and slip values were far from the ultimate value, so the change in the force–slip curves of the studs was not obvious, and the influence on the constitutive parameters of the elastic connection unit in the finite element model was weak, so it had little influence on the overall bending performance of the composite beams. In addition, the pull-out effects of the studs were not considered in the finite element analysis, which could also have been influential in the above results.

5. Conclusions

Three analyses methods—the push-out test, the beam test, and finite element analysis—were used to systematically study the effects of concrete strength (C30, C40, and C50), stud diameter (13, 16, and 19 mm), and stud height (60, 90, and 120 mm) on the shear performance of headed studs and the flexural behavior of steel-concrete composite beams. The main conclusions are as follows:

(1) All push-out specimens were damaged by the shear fracture at the root of the studs. Compared with the 13 mm diameter stud, the 16 mm and 19 mm diameter stud's ultimate capacity increased by 27% and 48%, respectively. Improving the concrete strength (from C30 to C40) or the stud height (from 60 mm to 90 mm) within a certain range increased the shear capacity of the stud by approximately 10%; continuing to increase the concrete strength or stud height had little impact on the stud capacity.

(2) The failure modes of the composite beam were the bending failure of the pure bending section and shear failure at the fulcrums. The lower flange of the steel beam was the first to yield under the loading points. The distribution curves of deflection were close to parabolic along the beam length of the composite beam specimen. The relative slip at L/8 was the largest but did not exceed 1 mm, followed by the slip at the fulcrum and L/4, and the relative slip at 3L/8 near the mid-span was the smallest. Before 0.8 Pu, the studs could effectively transfer the force, and the cooperative stress performance of the concrete slab and steel beam was good. The stress of the section at L/2 of the composite beam conformed to the assumption of the plane section.

(3) The results of FEA based on the composite beam test showed that, among the studied parameters, the capacity of the composite beam was most obviously affected by the number of studs. Increasing the number of studs could increase the flexural capacity of the composite beam, but the growth rate of flexural capacity decreased gradually. Compared with only 2 studs, the yield load of the composite beam increased by 7%, 17%, and 26%, and the ultimate load increased by 10%, 23%, and 31% for models with 4, 8, and 16 studs, respectively. Increasing concrete strength had a certain effect on the increased capacity of the composite beams. According to our finite element model, changing the diameter or height of the studs had little effect on the flexural capacity of the composite beams when the studs reached a certain degree of connection.

Although some conclusions were drawn in this paper, there were also some limitations. For example, only one piece of simply supported steel-concrete composite beam was tested, and it is recommended to conduct multiple tests to investigate the effect of different stud parameters on the flexural performance of composite beams. In the finite element analysis, the elastic connection units were used to simulate the studs, which differed from the actual three-dimensional model, and it is recommended to use solid unit modeling and conduct fine simulations of the friction and bonding between the studs and concrete.

Author Contributions: Conceptualization, S.Z. and Y.J.; methodology, S.Z.; software, S.Z.; validation, S.Z.; formal analysis, S.Z.; data curation, S.Z. and Y.D.; writing—original draft preparation, S.Z.; writing—review and editing, S.Z., Y.J. and Y.D.; funding acquisition, Y.J. All authors have read and agreed to the published version of the manuscript.

Funding: This study was funded by the Natural Science Foundation of Heilongjiang Province of China, grant number E2017003.

Institutional Review Board Statement: Not applicable.

Informed Consent Statement: Not applicable.

Data Availability Statement: Not applicable.

Conflicts of Interest: The authors declare no conflict of interest.

References

1. Liu, Y.; Zeng, M.; Chen, A. Application and research of shear connectors in bridge structures. *J. Harbin Inst. Technol.* **2003**, *35*, 277–280. [CrossRef]
2. Viest, I.M. Investigation of Stud Shear Connectors for Composite Concrete and Steel T-Beams. *J. Am. Concr. Inst.* **1956**, *27*, 875–891.
3. Ollgaard, H.G.; Slutter, R.G.; Fisher, J.G. Shear strength of stud connectors in light-weight and normal weight-concrete. *AISC Eng. J.* **1971**, *8*, 55–64.
4. SHIM, C.S.; LEE, P.G.; YOON, T.Y. Static behavior of large stud shear connectors. *Eng. Struct.* **2004**, *26*, 1853–1860. [CrossRef]
5. Pallarés, L.; Hajjar, J.F. Headed steel stud anchors in composite structures, Part I: Shear. *J. Constr. Steel Res.* **2010**, *66*, 198–212. [CrossRef]
6. Pallarés, L.; Hajjar, J.F. Headed steel stud anchors in composite structures, Part II: Tension and interaction. *J. Constr. Steel Res.* **2010**, *66*, 213–228. [CrossRef]
7. Li, A.; Krister, C. Push-out tests on studs in high strength and normal strength concrete. *J. Constr. Steel Res.* **1996**, *36*, 15–29. [CrossRef]
8. Nie, J.; Tan, Y.; Wang, H. Strength of stud shear connectors in composite steel HC beams. *J. Tsinghua Univ. Sci. Technol.* **1999**, *12*, 94–97. [CrossRef]
9. Hu, Q.; Yang, C.; Huang, C.P. Study of Finite Element Simulation Method of Steel concrete Interface of Shear Studs Push- out Test. *J. Hubei Univ. Technol.* **2017**, *32*, 7–10+36. [CrossRef]
10. Huu, T.N.; Seung, E.K. Finite element modeling of push-out tests for large stud shear connectors. *J. Constr. Steel Res.* **2009**, *65*, 1909–1920. [CrossRef]
11. Wang, J.F.; Zhang, A.P.; Wang, W.H. Effects of stud height on shear behavior of stud connectors. *J. Zhejiang Univ. Eng. Sci.* **2020**, *54*, 2076–2084. [CrossRef]
12. Meng, H.; Wang, W.; Xu, R.Q. Analytical model for the Load-Slip behavior of headed stud shear connectors. *Eng. Struct.* **2022**, *252*, 113631. [CrossRef]
13. Wu, F.W.; Feng, Y.P.; Dai, J.; Wang, G.Q.; Zhang, J.F. Study on mechanical properties of stud shear connectors in steel-uhpc composite structures. *Eng. Mech.* **2022**, *39*, 222–234+243. [CrossRef]
14. Moffatt, K.; Lim, P. Finite element analysis of composite box girder bridges having complete or incomplete interaction. *Proc. Inst. Civ. Eng.* **1976**, *61*, 1–22. [CrossRef]
15. Xing, X. Mechanical Performance Analysis of H Section Steel-Concrete Composite Beams with Stud Connectors. Master's Thesis, Xiangtan University, Xiangtan, China, 2016.
16. Xiu, H.L.; Wang, J.Q.; Li, M. The comparative study of the load-slip relationship of stud connectors based on beam test and push-out test. *Steel Constr.* **2017**, *32*, 28–35. [CrossRef]
17. Wang, B.; Huang, Q.; Liu, X.; Li, W. Experimental investigation of steel-concrete composite beams with different degrees of shear connection under monotonic and fatigue loads. *Adv. Struct. Eng.* **2018**, *21*, 227–240. [CrossRef]
18. Zhang, J.; Hu, X.; Fu, W.; Du, H.; Sun, Q.; Zhang, Q. Experimental and theoretical study on longitudinal shear behavior of steel-concrete composite beams. *J. Constr. Steel Res.* **2020**, *171*, 4. [CrossRef]
19. Sangeetha, P.; Gopal, S.R.; Vigneshwar, A.J. Flexural Strength of Steel-Concrete Composite Beams Under Two-Point Loading. *Civ. Environ. Eng. Rep.* **2020**, *30*, 21–32. [CrossRef]
20. Ding, F.X.; Wang, E.; Lü, F.; Wang, L.; Yu, Y.; Huang, Q.; Yu, Z. Composite Action of steel-concrete composite beams under lateral shear force. *Eng. Mech.* **2021**, *38*, 86–98. [CrossRef]
21. *EN 1994-1-1*; Design of Composite Steel and Concrete Structures-Part 1-1: General Rules and Rules for Buildings. European Committee for Standardization: Brussels, Belgium, 2004.
22. *JTG 3362*; Specifications for Design of Highway Reinforced Concrete and Prestressed Concrete Bridges and Culverts. China Communications Press Co., Ltd.: Beijing, China, 2018.
23. *GB 10433*; Cheese Head Studs for Arc Stud Welding. Standards Press of China: Beijing, China, 2002.
24. JSSC. *Japanese Society of Steel Construction. Standard on Push-Out Test for Headed Stud (Draft)*; Japanese Society of Steel Construction: Tokyo, Japan, 1996.